

Flotation bubble size distribution detection based on semantic segmentation

Lei Zhang, Degang Xu

**School of Automation, Central South University, Hunan 410083, China (e-mail:dgxu @csu.edu.cn)*

Abstract: In mineral foam flotation, characteristic information of bubble images is closely related to the flotation process condition and production indicators, among which the bubble size distribution is a key feature. Therefore, accurately obtaining the bubble size distribution is of great significance for optimizing and controlling the flotation process. Froth segmentation is the main technique to obtain bubble size information of flotation cells. In this paper, one semantic segmentation algorithm is adopted to segment flotation froth image, and a new froth segmentation algorithm based with improved U-Net is proposed. The experiment results indicate that the developed algorithm not only successfully solves the problem of over-segmentation and under-segmentation, but also improves the segmentation accuracy, which is suitable for different process conditions and lighting conditions.

Keywords: froth flotation, froth segmentation, semantic segmentation, bubble size distribution.

1. INTRODUCTION

In recent years, metal-producing companies have increased their investment in automation and technological innovation, embracing new opportunities to enable transformational change (Bascur O.A.(2019)). Froth flotation is an important industrial process for separating valuable from gangue minerals. Because of the complexity of the flotation process (Han et al. (2016)), it is not enough to depend mainly on the workers' observation of the froth. Besides, the froth is a rich source of information regarding the operational state of the flotation system. Hence, using machine vision instead of human vision to accurately get the shape information of the froth has been used widely (Tessier J. et al.(2007)), and a variety of features have been extracted from the froth images. It is shown as Fig.1.

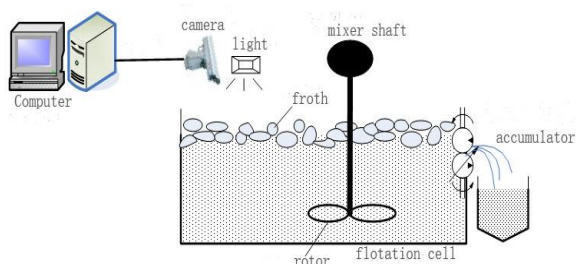


Fig.1. Monitoring of flotation based on machine vision

Among all the features, the distribution and shape of the froth are the direct expressions of the flotation conditions and production indicators (concentrate grade, tailing grade, etc.) (Moolman et al. (1996); Hosseini et al. (2014)). However,

accurately outlining the bubbles in the froth images is a challenging work due to several reasons. Froth image is composed of a large number of adhesive bubbles with weak edges which are difficult to detect. What's more, uneven distribution of bubble size and complex illumination in the scene environment are also problems of accurately segmenting froth image.

In the last few years, considerable attention has been paid to develop efficient and accurate algorithms for getting bubble size distribution in the froth images. The segmentation algorithm that has been proposed is mainly based on watershed segmentation algorithm, valley edge detection method and texture spectrum method.

Adaptive segmentation algorithm, combining fuzzy C-means and watershed algorithm to segment bubbles, and use fuzzy texture features to distinguish between over-segmentation and under-segmentation (Chen et al. (2011)). Then, a new watershed algorithm based on triple mark improved the efficiency of segmentation (Jahedsaravani A et al. (2011)). In this algorithm, three sets of markers are extracted from the froth image. The first set of markers is determined by using an adaptive thresholding. Two other sets of markers are extracted by applying some morphological operators followed by thresholding (using hard and soft threshold values). All sets of markers are eventually integrated and the watershed transform is applied. Recently, a new watershed algorithm based on whole and sub-image classification techniques is presented (Jahedsaravani A et al. (2017)). In this method, marker based watershed algorithm is integrated with a neural network classifier. Classification of the froth images based on the bubble size is applied before any further processing, which will effectively prevent over-segmentation and under-segmentation. These marker-based watershed segmentation methods are very sensitive to illumination conditions and difficult to segment accurately in edge blur conditions.

* This work was financially supported by the Australia-China Science and Research Fund 2016YFE0101300, by the National Natural Science Foundation of China under Grant 61973320 and 61473319.

Aiming at the weak edges problem in the froth images, a segmentation algorithm combining multi-scale edge enhancement and valley edge detection algorithms is proposed (Liao et al. (2016)). Zhou Kaijun proposed a method based on fuzzy three-valued bubble image edge detection (Zhou et al. (2014)). They only solved the problem of weak edges, without considering the uneven size of the froth and the influence of illumination.

As aforementioned, a froth segmentation algorithm that is generally applicable to scene environment is still absent. In recent years, deep learning is widely used in image

processing and show great advantages (Maier A et al. (2018)). Among them, the semantic segmentation based on full convolutional neural network have recently demonstrated exceptional performance in various deep learning approaches, and in some of these surpassing the human level (Garcia-Garcia A et al. (2017)). The most common semantic segmentation networks include FCN, SegNet, U-Net (Long J et al. (2014); Badrinarayanan V et al. (2015); Ronneberger O et al. (2014)). the state-of-the-art methods include FastFCN, Gated-SCNN (Wu H et al(2019); Takikawa et al(2019))).

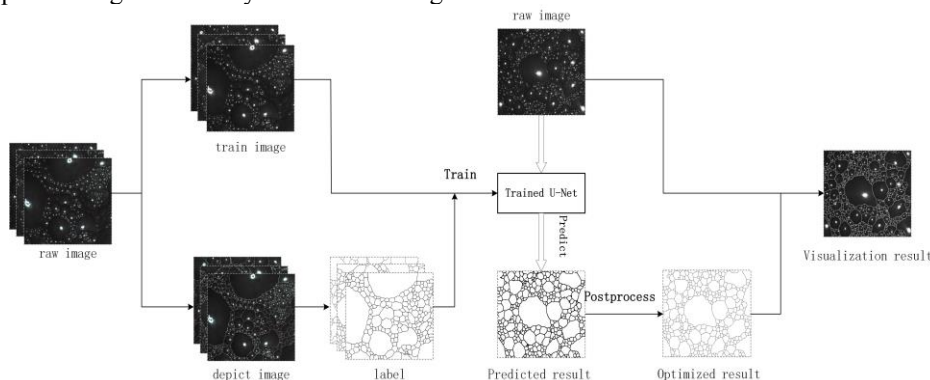


Fig.2. The flowchart of the proposed algorithm

A FCN-based network structure U-Net is selected as the main component of the method in the present study, firstly created by Ronneberger et al. and applied to biomedical image segmentation. The success of U-Net in biomedical image segmentation has fewer training images and more accurate result than CNN, driving the authors to study the application of U-Net in froth segmentation. In this paper, flotation froth image segmentation data set was built firstly by manual. Then, we use the improved U-Net network to train and get predictions. During training, data augmentation is applied to expand the data set. Finally, in order to optimize the results of the final depiction of the froth, refinement and filtering operations are followed the prediction. A schematic of proposed algorithm in this study is shown in Fig.2. To the best of author's knowledge, the approach proposed in this paper is the first time to consider the segmentation of froth image with deep network U-Net.

The main works of this paper are in the following four aspects. Firstly, we built a dataset for froth image segmentation, which has never been done before. Secondly, the long-standing difficulties of over-segmentation and under-segmentation have been conquered. Thirdly, the algorithm presented in this paper overcomes the complex environment on site and is suitable for a variety of working conditions. The other is adding Dropout layer into U-NET network, which can speed up training, prevent over-fitting.

2. DATA SET

2.1 Get data and make data set

A dataset of 35 images of the flotation froth is used. Raw froth images were collected with experimental facilities from a flotation plant in China. Experimental setup consists of

RGB camera with resolution of 1440x1200 and lens of 35 mm, high frequency variable light source, protection cover, fan protecting camera from water vapor and high temperature, optical fiber with length over 100m for signal communication to industrial PC computer in operating room.

In the dataset, the original image was stored as 8-bit grey scale images with a spatial resolution of 512×512 pixels. The ground truths were binary images representing the contours of the bubbles drawn manually. During training, the ground truths were used to train the network to recognize the bubble borders. There are also some ground truths in the testing set that are used to evaluate the performance of the model.

2.2 Data Augmentation

As for our research, it is difficult to obtain a larger amount of annotated images, so we use data augmentation by applying elastic deformations to the existing training images. This allows the network to learn some features that are not included in existing training set. In case of flotation froth image, we primarily consider shift and rotation invariance. This method is particularly useful in the froth image segmentation, since deformation of the froth is the most common variation during flotation, that is to say the realistic deformations can be simulated efficiently. The value of data augmentation has been proved in the scope of unsupervised feature learning (Dosovitskiy et al. (2014)).

In addition, we extend the data set by multi-scale transformation during training, an example is shown in Fig.3. First of all, multi-scale transformation is performed on the raw image. Then, for larger scale image, crop an area of the same size as the raw image. For smaller scale image, the

image is centered and filled around to the original image size. At the same time, the same operation is applied to the corresponding label.

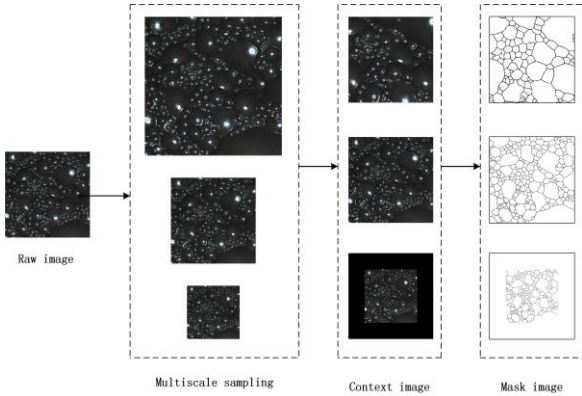


Fig.3. Extend data sets with multiscale transformations

3. PROPOSED METHOD

3.1 U-Net network structure

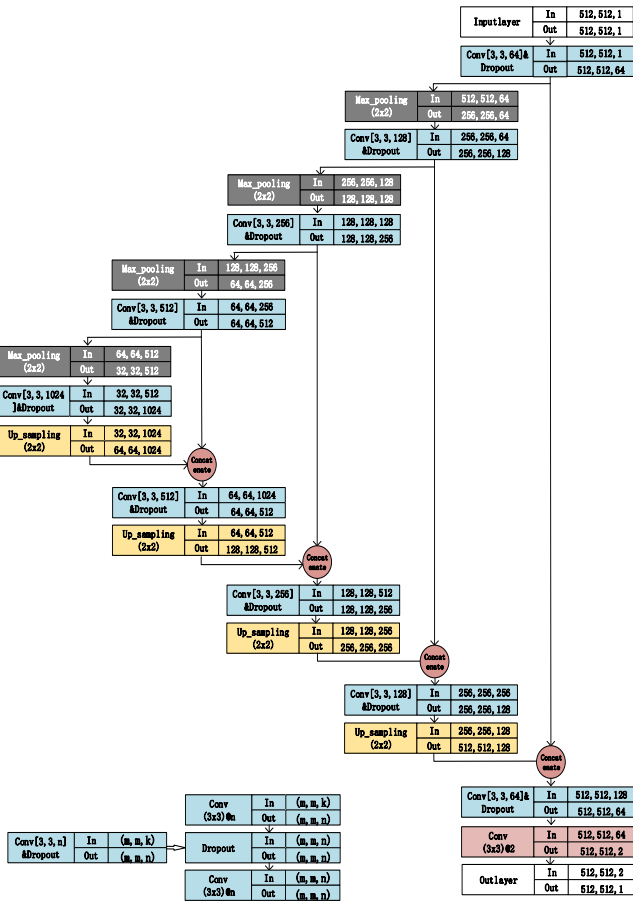


Fig.4. U-Net framework

U-Net network is evolved from a full convolution network and has a good performance at small dataset, which is also in the case of the dataset considered in this research. In the network, the symmetrical structure of the encoder and the decoder formed the elegant U type. Fig.4 shows the U-Net framework used in this study. The encoder extracts features by convolution, pooling, etc., and gradually reduces the input

data spatial dimension, while decoder regains the detailed features by feature fusion, deconvolution. As a result, it produces a pixel-level probability map.

The convolution layer use multiple sets of kernels of size 3x3 with a stride of 1 pixel for extracting features. In the convolution operations, full-zero padding strategy is adopted to conserve image boundary information and to make the output size the same as the input size.

Each convolution followed by a rectified linear unit (ReLU), and a commonly used activation function in neural networks, the use of which can adapt the network to more nonlinear functions (Glorot X et al. (2010)). To compare with sigmoid, ReLU function has unilaterally suppressed output, lager excitatory boundary, spares activation of the underlying network, and it does not have the problem of gradient disappearing. Hence, the network trained with ReLU function has a faster convergence rate than the network using Sigmoid function. ReLU is defined as (1).

$$ReLU(x) = \max(0, x) \quad (1)$$

Then, a max pooling layer of size 2x2 with stride 2 is used to future process the features. Through the max pooling operation, the feature dimension is reduced to half, the number of parameters is compressed, and over-fitting can be improved.

Overfitting is a serious problem in the deep neural nets with large number of parameters, so dropout layers (Srivastava N et al. (2014)) were introduced between the convolution layers to address this problem. The key idea is to stochastically drop the unit from the neural network during training, which prevents units from co-adapting too much. During training, dropout samples from different “thinned” networks. The standard network and dropout network diagrams are shown in Fig.5.

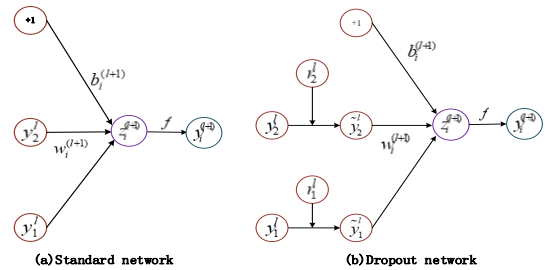


Fig.5. The comparison between standard network and dropout network

Decoder is similar to encoder, except that upsampling is used instead of max-pooling. In order to localize, high resolution features from the encoder path are combined with the upsampled output through concatenate operation. After that, convolution layer can learn to assemble a more precise output based on this information. The last convolutional layer is followed by a softmax activation layer which generates probability map.

3.2 Training

Loss function

The loss function describes the degree of deviation between the prediction and the truth in the training process. The smaller the difference between the prediction and the truth, the smaller the loss function, and as an optimization target that directly relates to the quality of the model training. For segmentation works, common loss functions include Dice loss function, cross entropy loss function, Focal loss function and the others.

The sample imbalance phenomenon exists in the flotation froth image. Sample imbalance means that the proportions of different classes of samples vary greatly in the classification learning algorithm, and a certain class in a train set occupies most of the proportion is called a simple sample. The large number of simple samples will lead to the large loss of the entire train set. For the flotation froth image in this study, the background is a simple sample and may have an absolute advantage over the loss function. Therefore, Focal loss(Lin et al. (2017)) function is selected to solve the sample imbalance problem in this paper, which is based on the cross entropy loss function. It can be described as(2).

$$FL(p) = \begin{cases} -\alpha \cdot (1-p)^\gamma \log(p) & \text{if } y = 1 \\ -\alpha \cdot (p)^\gamma \log(1-p) & \text{otherwise} \end{cases} \quad (2)$$

The above $y \in \{\pm 1\}$ specifies the ground-truth class, $p \in [0,1]$ is the model's estimated probability for the class with label $y = 1$, and $\gamma \geq 0$ is tunable focusing parameter, which can reduce the loss of simple sample, the parameter α represents the sample imbalance coefficient.

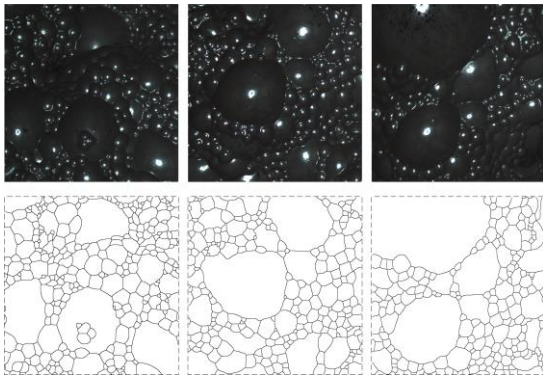


Fig.6. Examples of training sets. The first row: raw image, the second row: labeled image

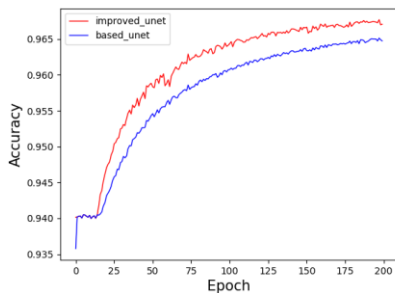


Fig.7. The accuracy curves during training

Ultimately, the proposed U-Net network was trained with training set. While training the Adam algorithm was applied

to optimize the model. Every time, the network was trained for 200 epochs which took about 3.5h. Examples of training sets and accuracy curves during training are shown in Fig.6 and Fig.7. We can find the improved U-net has higher accuracy compared with based U-net. The entire training process is performed on a workstation. (CPU: Intel Xeon(R) W-2123 @ 3.6Hz, RAM:16GB, GPU: Nvidia Geforce 2080ti).

3.3 Prediction and Postprocessing

The trained network was then applied in the testing sets to generate the predicted results. For a single test image, it just took less than 1 s. However, the edge contours outputted by the network is not one-pixel-wide, and there are some isolated points or short lines resulting from mis-segmentation. To solve these problems, the prediction results are followed by postprocessing operations which shown in Fig.8.



Fig.8. Flow chart of postprocessing operation

Firstly, using erosion operation to optimize the depiction of some weak boundaries. Then, the one-pixel-wide edge skeleton was extracted through optimized DLMA (Discrete λ -Medial Axis) algorithm (Hu et al. (2017)). Fig.10(a) present the connection of the inconsecutive contours by above operation. In the end, we design a non-boundary filter operator to filter out isolated points, line segments, and bifurcation lines in the image. Fig.9 is a 3x3 filter operator window.

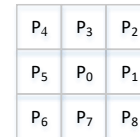


Fig.9 Filter operator window

P₀ is the pixel to be filtered, P₁~P₈ are the eight neighborhoods of P₀ with a value of 0 or 1, where 0 is the foreground and 1 is the background. The window filter operator is defined as follows:

$$P = \sum_{i=1}^8 P_i \quad (3)$$

And for the refined image, $P \in \{0,1,2,3\}$. The specific implementation of the operator is as follows:

(1) if $P \leq 1$:

$$P_0 = 0;$$

(2) if $P = 2$, define the operator as:

$$L = \sum_{i=1}^8 P_i P_{i+1} \quad (4)$$

where $P_9 = P_1$.

$$P_0 = \begin{cases} 1 & \text{if } L = 0; \\ 0 & \text{if } L = 1; \end{cases}$$

(3) if $P = 3$, define the operator as:

$$L = \sum_{i=1}^8 P_i P_{i+1} P_{i+2} \quad (5)$$

where $P_9=P_1, P_{10}=P_2$.

$$P_0 = \begin{cases} 1 & \text{if } L = 0; \\ 0 & \text{if } L = 1; \end{cases}$$

The result of filtering the refined image using this operator is shown in the Fig.10(b).

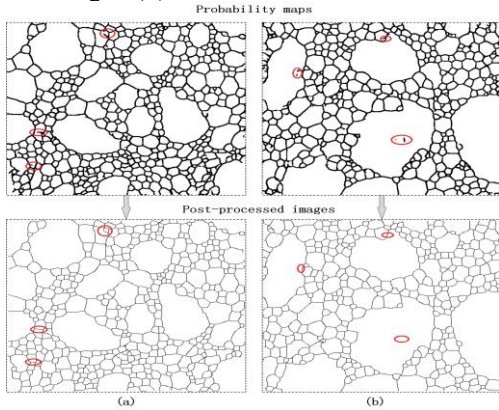


Fig.10. Comparison between probability maps and post-processed images.

4 RESULT AND COMPARISON

In this section, a set of new froth images that were never used in training set is used to test the performance of the trained model. Besides, the segmentation results of method in this paper are compared with the results of adaptive watershed algorithm.

The results from the three methods for three images under different working conditions are shown in Fig.11. Ground truth (A_1, B_1, C_1) is the label drawn by manual; Watershed (A_2, B_2, C_2) represent the segmentation result of adaptive watershed algorithm; Proposed (A_3, B_3, C_3) represent the segmentation result of the algorithm proposed in this paper. Distinctly, the problem of over-segmentation and under-segmentation that exist in adaptive watershed algorithm is disappeared in our proposed method.

Further more, the comparison of segmentation accuracy is shown in Figure 12. The first column is original picture, the watershed+truth presents a comparison of the segmentation of adaptive watershed algorithm (green line) with the manual segmentation (red line), the proposed+truth presents a comparison of the segmentation of proposed method (green line) with the manual segmentation (red line). We can find that the segmentation result of the proposed method is very close to the result of manual segmentation.

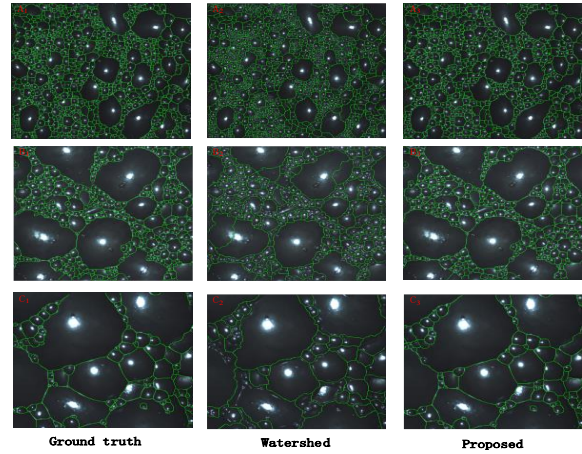


Fig.11. The results from the two methods for three images under different working conditions

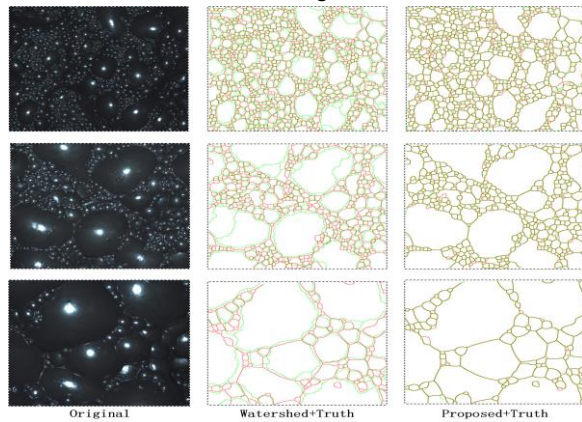


Fig.12. The comparison of segmentation accuracy

To quantify the accuracy of the proposed algorithm, the statistical information and size distribution information of flotation bubbles are presented in Fig.13. (a) is the comparison between detected number and ground truth number of bubbles. (b), (c) and (d) are bubble size distribution graph under different case.

Besides, the relative error of the algorithm in segmentation of the froth images were calculated from the expression:

$$E_r = \frac{x - x_0}{x} \quad (6)$$

where E_r is the relative error, x is the actual mean bubble size get from the manual segmentation (pixel) and x_0 is the mean bubble size measured by the automatic segmentation (pixel). The error values of the algorithm in delineation of images are listed in Table 1.

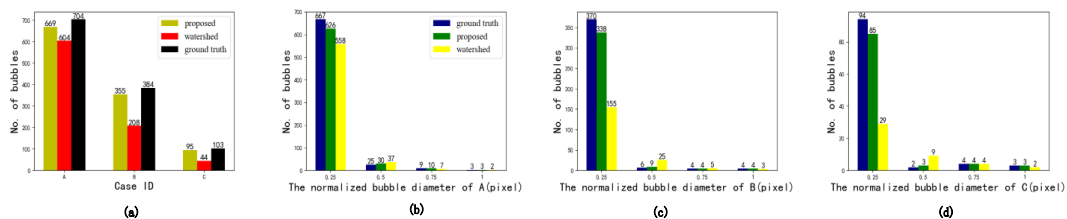


Fig.13. The assessment of the determined number of bubbles; (a) detected number and ground truth number comparison; (b), (c), (d) the bubble size distribution.

Table 1. Relative error of the developed algorithm in segmentation of froth images.

image	Manual segmentation	Watershed		U-net	
	x	x_0	$E_r(\%)$	x_0	$E_r(\%)$
A	53.07	56.98	-7.36	55.68	-4.9
B	62.36	67.93	-8.93	63.72	-2.18
C	122.62	140.21	-14.34	123.70	-1.08

5 CONCLUSIONS

In this paper, we focus on the problem of flotation froth image segmentation, a new froth segmentation algorithm based on improved U-Net is proposed. It is the first time that a semantic segmentation approach which based on deep learning has been applied to this field. The performance of the proposed algorithm is tested in the paper and compared with the traditional adaptive watershed algorithm.

The results indicate that the algorithm not only successfully solves the problems of over-segmentation and under-segmentation, but also improves segmentation accuracy. Accurate segmentation of froth images result in accurate flotation bubble size distribution, which provides more accurate and effective guidance for field workers' work; and the robust performance of the proposed algorithm enables long-term stable operation of monitoring. This is of great significance for reducing work intensity and increasing production efficiency.

REFERENCES

- A. Jahedsaravani, M. Marhaban, M. Massinaei, M. Saripan, N. Merhad, S. Noor, Development of a new algorithm for segmentation of flotation froth images, *Miner. Metall. Process. J.* 31 (2014) 66–72
- Badrinarayanan V, Handa A, Cipolla R. SegNet: A Deep Convolutional Encoder-Decoder Architecture for Robust Semantic Pixel-Wise Labelling[J]. *Computer Science*, 2015.
- Bascur O A, Soudek A. Grinding and Flotation Optimization Using Operational Intelligence[J]. *Mining, Metallurgy & Exploration*, 2019, 36(1): 139-149.
- Chen X F, Gui W H, Yang C H, et al. Adaptive image processing for bubbles in flotation process [J]. *Measurement & Control*, 2011, 44(4) : 121 - 125 .
- Dosovitskiy A, Springenberg J T, Riedmiller M, et al. Discriminative Unsupervised Feature Learning with Convolutional Neural Networks[J]. 2014.
- Glorot X , Bordes A , Bengio Y . Deep Sparse Rectifier Neural Networks[C]// Proceedings of the 14th International Conference on Artificial Intelligence and Statistics (AISTATS). 2010.
- Garcia-Garcia A, Orts-Escolano S, Oprea S, et al. A review on deep learning techniques applied to semantic segmentation[J]. 2017.
- Hu Yan, Wang Ping. Skeleton Extracting Algorithm via Optimized Discrete λ -Medial Axis[J]. *Journal of Computer-Aided Design & Computer Graphics*, 2017, 29(8):1505-1514.
- Han J., Yang C., Zhou X., et. al. Entropy-based estimation of bubble size distributions in froth flotation using B-spline functions[J]. *IFAC-PapersOnline*, 2016, 49(20):69-101.
- Jahedsaravani A, Massinaei M, Marhaban M H. An Image Segmentation Algorithm for Measurement of Flotation Froth Bubble Size Distributions[J]. *Measurement*, 2017, 111.
- Long J, Shelhamer E, Darrell T. Fully Convolutional Networks for Semantic Segmentation[J]. *IEEE Transactions on Pattern Analysis & Machine Intelligence*, 2014, 39(4):64 0-651.
- Liao Y P, Wang W X. Flotation froth images segmentation based on multiscale edge enhancement and adaptive valley detection[J]. *Optics and Precision Engineering*, 2016, 24(10):2589-2600.
- Lin T Y, Goyal P, Girshick R, et al. Focal Loss for Dense Object Detection[J]. *IEEE Transactions on Pattern Analysis & Machine Intelligence*, 2017, PP (99):2999-3007.
- Moolman D W, Aldrich C, Schmitz G P J, et al. The interrelationship between surface froth characteristics and industrial flotation performance[J]. *Minerals Engineering*, 1996, 9(8):0-854.
- M. Hosseini, H.H.A. Shirazi, M. Massinaei, N. Mehrshad, Modeling the relationship between froth bubble size and flotation performance using image analysis and neural networks, *Chem. Eng. Commun.* (2014).
- Maier A, Syben C, Lasser T, et al. A Gentle Introduction to Deep Learning in Medical Image Processing[J]. 2018.
- Ronneberger O, Fischer P, Brox T. U-Net: Convolutional Networks for Biomedical Image Segmentation[J]. 2015.
- Srivastava N, Hinton G, Krizhevsky A, et al. Dropout: A Simple Way to Prevent Neural Networks from Overfitting[J]. *Journal of Machine Learning Research*, 2014, 15(1):1929-1958.
- Tessier J, Duchesne C, Bartolacci G. A machine vision approach to on-line estimation of run-of-mine ore composition on conveyor belts[J]. *Minerals Engineering*, 2007, 20(12):1129-1144.
- Takikawa, Towaki, Acuna, David, Jampani, Varun et al. Gated-SCNN: Gated Shape CNNs for Semantic Segmentation[J]. 2019
- Wu H , Zhang J , Huang K , et al. FastFCN: Rethinking Dilated Convolution in the Backbone for Semantic Segmentation[J]. 2019.
- Zhou K J, Gui W H, Yang C H. Mineral flotation froth image edge detection method based on fuzzy ternary pattern[J]. *Chinese Journal of Electronics*. 2014, 42(4):658-665.